Detection of VLF attenuation in the Earth-ionosphere waveguide caused by X-class solar flares using a global lightning location network

T. S. Anderson[1], M. P. McCarthy[1], and R. H. Holzworth[1]

[1]Department of Earth and Space Sciences, University of Washington.

Corresponding author: Todd S. Anderson (tshelbya@uw.edu)

Key Points:

- VLF lightning location network detection efficiency is severely impacted by powerful solar flares and other space weather events.
- By comparing the current stroke-to-station path distribution with a background distribution, VLF attenuation regions can be detected.
- This technique enables near-real-time VLF attenuation and ionosphere parameter monitoring in the Earth-ionosphere waveguide.

Abstract

Solar flares, energetic particles and Earth-impacting coronal mass ejections enhance ionization in the lower ionosphere, inhibiting radio wave propagation in the Earth-ionosphere waveguide (EIWG). This enhanced ionization is observed locally by ionosondes and GPS/GNSS receivers, but spatial coverage of these observations is limited by receiver location. VLF propagation studies have previously been performed to assess the impact of space weather on the EIWG; however, these studies are typically limited by small numbers of fixed VLF transmitters and receivers, and observe only the region of the EIWG along propagation paths between transmitters and receivers. Here, we use global lightning as a VLF source, and an existing lightning detection network as a receiver. By mapping sferic propagation paths between lightning strokes and numerous network stations, and considering how this distribution of paths changes during solar events, we can identify attenuation regions in the EIWG caused by space weather. We describe the VLF response in the EIWG to two X-class solar flares, and compare mapped attenuation regions with those provided by the NOAA D-Region Absorption Prediction (D-RAP) model. The identified attenuation regions associated with these flares match the D-RAP-predicted regions well in both spatial extent and onset timing. Measurements of VLF attenuation caused by solar flares can provide ground-truth confirmation of modeled attenuation, and can inform the detection efficiency of lightning location networks. This analysis also paves the way for real-time VLF attenuation mapping in the EIWG.

Plain Language Summary

Very-low-frequency (3-30 kHz, “VLF”) radio signals can propagate long distances by reflection between the ground and the lower ionosphere. This property enables the detection and location of lightning strokes, which emit radio waves in a large frequency band, with relatively few VLF receiver stations positioned around the world. Solar flares, and other space weather events, can severely reduce the propagation distance of VLF waves around the Earth, limiting the effectiveness of lightning location networks and disrupting other infrastructure that relies on radio wave interaction with the lower ionosphere. We present a technique for detecting VLF attenuation using a lightning location network. This study improves our understanding of the effects of solar flares on lightning detection, and provides the groundwork for a lightning detection network to be used as a real-time monitor of radio attenuation in the lower ionosphere.

1 Introduction

Solar extreme ultraviolet (EUV) radiation generates most of Earth’s ionosphere; and changes in the energetic particle and radiation output of the Sun can dramatically affect the Earth’s ionosphere profile. Solar flares enhance ionization on short timescales, which significantly alter the ionosphere density profile throughout even the lowest layers (e.g. Mitra, 1974). This enhanced ionization in the D region can severely impact VLF radio wave propagation in the Earth-ionosphere waveguide (e.g. Thomson & Clilverd, 2001).

Mapping D-region ionosphere density at the global scale and with high time resolution is challenging and often involves using both ground-based radio propagation measurements and in-situ instrument campaigns. Ionosondes and GPS/GNSS TEC measurements can produce accurate profiles of the E- and F-region ionosphere, but usually cannot resolve D-region electron density and are effective only over ground stations. Long-duration in situ measurements are difficult in this altitude band; the D region, at 50-80km altitude, is too high for stratospheric balloons, but thermosphere drag precludes long-duration orbital measurements there. VLF monitoring stations or networks can characterize propagation along transmitter-to-receiver paths; however, such networks operating today rely on a small number of transmitters (e.g. MSK stations) and receivers, and therefore suffer from poor spatial resolution of regional ionosphere features (e.g. Chilton, Steele, & Norton, 1963; Crombie, 1965; Thomson & Clilverd, 2001; Bouderba, NaitAmor, & Tribeche, 2016). By using global lightning as a VLF source, we can detect regional VLF attenuation features with higher spatial and temporal resolution.

Previous work by other authors has shown that the Wait and Spies 2-parameter ionosphere (e.g. Thomson, N., 1993) can be inferred from measurements of lightning-launched sferics. Cummer, Inan, and Bell (1998) compared modeled and measured VLF and ELF sferics to infer nighttime D region electron density. Jacobson, Holzworth, Lay, Heavner, and Smith (2007) demonstrated a method of lower-ionosphere sounding by opportunistic use of LF sferics launched by Narrow Bipolar events. Jacobson, Shao, and Holzworth (2010) reported on a steep-incidence VLF/LF sounding method for studying transient, localized disturbances in the nighttime D region. Carvalho, et al. (2017) presented a method to measure the ionospheric effective reflection height along 200-250km paths from VLF sferics launched by triggered lightning. Gross, Cohen, Said, and Gołkowski (2018) used MSK transmitter stations as well as lightning sferics to infer ionosphere parameters from polarization of VLF signals, and McCormick, Cohen, Gross, and Said (2018) calculated ionosphere parameters using a comparison of simulated and measured sferics from several thunderstorms; both these techniques were presented for continent-scale regions, with possible extensions to global coverage in future work. A technique to provide a large-scale D region diagnostic using a small number of receivers to measure ELF sferic group velocity was presented by Gołkowski, et al. (2018). Thus far, a real-time global lower ionosphere monitor has not been demonstrated.

1.1 Lightning-generated sferics in the Earth-ionosphere waveguide

Cloud-to-ground lightning strokes typically discharge voltages of >1 MV over ~70 μs, with peak current in the 10-100 kA range (Uman & Krider, 1982). Each lightning stroke can be thought of as a short-lived transmission line antenna that emits broad-spectrum electromagnetic waves in a dipole-like radiation pattern. These radio waves are reflected by the lower ionosphere at an altitude where their frequency matches the electron plasma frequency ω_{pe} (e.g. Parks, 2004):

$$\omega_{pe}^2 = \frac{n_e e^2}{m_e \epsilon_0}$$

Where n_e is the electron number density, e is the electron charge, m_e is the mass of the electron and ϵ_0 is the permittivity of free space. The lower ionosphere acts as a reflector to radio waves in the ELF (3-3000Hz) and VLF (3-30kHz) frequency range. For a given frequency ω, the ionosphere can be thought of as a conductive spherical shell. Earth's surface, having electrical conductivity much greater than the intervening atmosphere, forms a conductive inner shell (e.g. Siingh, et al., 2007). Together, the lower ionosphere-atmosphere-Earth surface forms the Earth-ionosphere waveguide (EIWG), through which ELF and VLF radio waves may propagate long distances. VLF waves launched by lightning strokes that propagate in the EIWG are called atmospheric waves, or sferics.

By detecting sferic wave packets that propagate large distances in the EIWG, we can observe global lightning with a relatively small number of observing stations. The World Wide Lightning Location Network (WWLLN) is a network of ~80 stations, distributed globally between ±80° latitude. Each station listens for sferics and reports the time of group arrival (TOGA) to a processing server; this server then combines TOGAs from each detecting station, and determines the location and time of the lightning stroke (Dowden, Brundell, & Rodger, 2002), (Dowden, et al., 2008), (Hutchins, et al., 2012).

1.2 Impact of solar flares on radio attenuation in the EIWG

Increased X-ray and EUV flux from solar flares has been shown to enhance ionization in the lower ionosphere (e.g. Mitra, 1974). This electron density enhancement at low altitudes lowers the reflection altitude of radio waves propagating in the EIWG, including lightning-launched sferics. Because of increased neutral particle density at lower altitudes, more energy is lost to electron-neutral collisions during radio wave reflection, and hence the wave is more attenuated while ionization in the lower ionosphere is enhanced.

Using near-real-time lightning location information from WWLLN, we can detect VLF attenuation in the EIWG caused by solar flares. By leveraging the spatial distribution of WWLLN network stations, we can approximately map VLF attenuation regions on timescales of ~10 minutes.

Detection of attenuation regions relies on differing timescales of solar flares and thunderstorms. Thunderstorm flash rate and geographic location typically vary on the order of hours (Rakov & Uman, 2003), while solar flare onset typically occurs in minutes and X-ray irradiance decays by an order of magnitude within ~1 hour (Codrescu, Mihail; NOAA Space Weather Prediction Center, 2010). Enhanced low-altitude ionization from solar flare activity will occur in a circular region centered on the Earth subsolar point (Sauer & Wilkinson, 2008), (Levine, Sultan, & Teig, 2019).

In addition to increased attenuation in the lower-frequency portion of the VLF band (<10 kHz), solar flares can cause enhancement of VLF signals in the higher-frequency VLF (>15 kHz) (Volland, 1995). Such enhancements have been observed recently by Wenzel et al. (2016), which used four receivers in Europe and North America to measure amplitude and phase changes in VLF transmitter signals during M- and C-class flares; and George et al. (2019), which measured amplitude enhancements in the NPM 21.4 kHz signal using a receiver at Scott Base, Antarctica, during several X-class solar flares. Since WWLLN uses the <16 kHz portion of VLF sferics to locate lightning strokes, it is sensitive to VLF attenuation caused by solar flares, but not enhancement in the higher-frequency VLF.

The method presented here for detection of solar flare effects relies on the decrease of WWLLN detection efficiency near the subsolar point. This means the network, like other VLF lightning detection networks, is adversely affected by ionizing events from space, and these modifications to the network affect interpretations of lightning data. By studying the impact of solar flares on WWLLN lightning detection, we can improve our understanding of the effects of space weather on lightning detection networks and other technologies that rely on VLF reflection in the EIWG.

2 Methods

2.1 Global lightning stroke-to-station path distribution

WWLLN detects 0.5-1.5 million lightning strokes per day. These stroke locations are processed in real time, and by plotting great circle paths between stroke locations and the stations that detect each stroke, we can build a global stroke-to-station path distribution with a 10-minute timestep. A stroke-to-station path distribution for a 10-minute time window ending at time t is notated here as $ss(t)$: a matrix of integers, where each element counts the number of stroke-to-station path crossings of the geographic area that element represents. We chose 1° latitude/longitude grid regions, such that $ss(t)$ has 180×360 elements that cover the Earth and do not overlap. A sample stroke-station path distribution for a 10-minute time window is shown in Figure 1.

Grid locations near high-quality WWLLN stations or active thunderstorm regions typically are traversed by 10^3-10^4 stroke-station paths every ten minutes, whereas locations near the poles or far from both WWLLN stations and active thunderstorms may be traversed by only a few stroke-station paths per day. Ground composition along the path is also important; since ice is much less conductive than dry land or ocean water, sferic propagation across the North pole is only possible via a few ocean routes, and propagation across Greenland and Antarctica is rare (Westerlund & Reder, 1973), (Barr, Jones, & Rodger, 2000).

2.2 Model comparison: D-Region Absorption Prediction

We used the NOAA D-Region Absorption Prediction (D-RAP) model to inform our guess for VLF attenuation region geometry and timing (Codrescu, Mihail; NOAA Space Weather Prediction Center, 2010). The D-RAP model predicts HF radio attenuation using X-ray, electron and proton flux detected by the GOES constellation. Absorption at the subsolar point is calculated with an empirical relation between the highest affected frequency (HAF) and X-ray flux (Sauer & Wilkinson, 2008):

$$HAF\ (\mathrm{MHz}) = (65 + 10\log_{10}[flux\ (\mathrm{W\ m^{-2}})])\ (\cos\chi)^{0.75}$$

Where χ is the solar zenith angle. For example, the HAF for an X9.3 flare (*flux* = 9.3×10^{-4} W m^{-2}) is about 35 MHz, decaying to 0 at the day/night terminator.

Although the D-RAP model addresses HF, not VLF, attenuation in the EIWG, it is still a useful comparison for a VLF attenuation analysis. HF and VLF attenuation in the EIWG during solar flares are both primarily caused by increased low-altitude ionization, and thereby increased electron-neutral collision frequency during wave reflection. Hence, both D-RAP and this VLF attenuation analysis are addressing changes in the lower ionosphere that should be approximately collocated and simultaneous.

2.3 Attenuation region visualization

We can gain insight into spatial and temporal variation in EIWG parameters by looking for changes in the global stroke-station path distribution through time. Energetic solar flares are particularly useful events to study, because of their predictable ionization enhancement in the lower ionosphere. With the assumption that far-field solar flare radiation can be treated as a planar radiation packet that is not appreciably distorted by Earth's magnetic field, nor does it contain fine structure relative to the size of the Earth, the pattern of enhanced ionization in the lower ionosphere is a circular region centered on the subsolar point (Codrescu, Mihail; NOAA Space Weather Prediction Center, 2010), (Levine, Sultan, & Teig, 2019).

We can use the WWLLN stroke-station path distribution to look for VLF attenuation regions in the EIWG. First, we identify a background stroke-station path distribution at the time just before flare onset. Next, we measure the stroke-station path distribution immediately following flare onset, and calculate attenuation of stroke-station paths relative to the background distribution.

A background stroke-station path distribution is generated by taking the median of several consecutive stroke-station path distributions during a period of quiet solar activity. For any time t, a background distribution is constructed by taking the median of the previous hour's stroke-station path distributions,

$$ss_b(t) = \text{Median}(\{ss(t_i)\}_{i=1}^{6})$$

For a 1° latitude-longitude grid, ss_b is a 180 x 360 matrix, where each element is the median number of stroke-station paths crossing that grid location in the set of 10-minute time intervals ending at $t_i = (t - i \times 10 \text{ minutes})$. This time interval ranges from $t - 70$ minutes to $t - 10$ minutes; it is the hour preceding the 10-minute interval covered in $ss(t)$.

The 10-minute sample size is chosen because it is short enough to capture the onset of solar flare ionization, while still containing a large population of stroke-station paths. Additionally, WWLLN writes files containing stroke-station path and stroke power information every 10 minutes, so this is a convenient duration for a real-time analysis. A 1-hour median timescale was chosen to be shorter than typical mesoscale convective system lifetime (Markowski & Richardson, 2011), while acknowledging that individual thunderstorm flash rate can vary significantly minute-to-minute. A longer median timescale would reduce the median distribution's relevance to t as an immediate background, while a shorter median timescale would be more susceptible to varying thunderstorm flash rate.

Next, the 10-minute stroke-station path distribution immediately following a solar flare is compared to the last hour's background stroke-station path distribution. Solar flare times are identified as peaks in GOES-13 X-ray irradiance data (NOAA NCEI, 2019). VLF attenuation regions can be characterized by the attenuation $\mathcal{A}$, in decibels, of stroke-to-station paths,

$$\mathcal{A}(t) = 10 \log_{10}\left(\frac{ss(t)}{ss_b(t)}\right)$$

This measure of VLF attenuation is only accurately defined at matrix locations with sufficient counts in both matrices; it is most accurate at geographic locations near WWLLN stations and/or frequent thunderstorm regions.

Additionally, we can validate attenuation region timing by computing the characteristic size of VLF attenuation region, and comparing the change of the size of this region with geostationary X-ray flux data (NOAA NCEI, 2019). We correlate X-ray flux recorded by the GOES-13 satellite with the size of the largest circular contour centered on the subsolar point within which the average stroke-station path attenuation exceeds 6 dB. This threshold can be tuned to accept attenuation regions generated by lower-power flares, but is particularly useful for observing the onset timing of large attenuation regions and the radial change in stroke-station path attenuation within the region.

3 Results and Discussion

In this analysis, we considered the X9.3 and X8.2 solar flares of September 6 and 10, 2017. The solar events of this period are well-studied (Yasyukevich, et al., 2018), (Gary, et al., 2018), (Qian, et al., 2019), (Levine, Sultan, & Teig, 2019). Sunspot group AR2673 produced several flares between late August and September 10, as well as solar energetic particles (SEPs) and coronal mass ejections (CMEs). Although these particle events had a significant impact on the ionosphere, this was mostly contained in the polar caps, and solar flare ionization was still the primary effect on the lower ionosphere at low- to mid-latitudes. Among several powerful solar flares originating from this sunspot group, we chose the X9.3 flare at 12:10 UT on September 6, and the X8.2 flare at 16:10 UT on September 10, because radio propagation in the low-latitude ionosphere was expected to be nominal in the hours leading up to flare onset, as predicted by D-RAP.

Attenuation in the EIWG caused by the solar flares of September 6 and 10, 2017, was investigated by plotting the attenuation in WWLLN stroke-station path crossings using a 10-minute timestep and 1-hour median baseline distribution. A comparison between the WWLLN response and the D-RAP predicted absorption is shown in Figure 2. A timing comparison between attenuation region radius and GOES-13 X-ray irradiance is shown in Figure 3. Finally, WWLLN stroke detection count rate for a sample 1000-km-radius region near the subsolar point during the September 10, 2017 flare is compared with GOES-13 X-ray irradiance in Figure 4.

Figure 2 shows comparisons between the D-RAP HAF maps and WWLLN-detected VLF attenuation. Figure times are chosen to reflect peak X-ray irradiance at flare onset; in the cases of both the September 6 and September 10 flares, maximum extent of both HF and VLF attenuation occurs within a few minutes of peak X-ray irradiance.

The September 6 flare at ~12:00 UT is preceded by an X-class flare at ~9:00 UT, and solar energetic particles (SEPs) that enhance ionization near the poles. The HAF map at 12:10 UT shows the subsolar attenuation region produced by the solar flare, but also polar attenuation regions produced by earlier and ongoing particle effects. The September 10 flare at ~16:00 UT is not immediately preceded by other powerful flares or SEPs, but SEPs are launched at the same time as the flare and arrive at the Earth within an hour of the peak X-ray irradiance. These generate polar attenuation regions as well.

The VLF attenuation regions mapped using WWLLN stroke-station paths closely match D-RAP-predicted HF attenuation regions at flare onset. For both the September 6 and 10 flares considered, the extent of 6dB median stroke-station path attenuation tracks that of ~10MHz 1dB absorption predicted by D-RAP, with the exception of polar attenuations, which are not captured by the WWLLN stroke-station path difference. It should be noted here that both D-RAP-predicted HF attenuation and VLF attenuation mapped here extend nearly to the terminator, which is the expected limit for attenuation caused by solar EM radiation.

Figure 3 shows that the onset timing of subsolar VLF attenuation regions occurs within this analysis' 10-minute time resolution of peak X-ray irradiance measured at GOES-13. X-ray irradiance peaked at 12:02 UT on September 6, 2017 and 16:03 UT on September 10; VLF-attenuation region radius on both these days peaked during the ten-minute intervals containing these times.

X-class flares have a significant impact on WWLLN detection of lightning strokes, as shown in Figure 4. Here, the WWLLN-detected occurrence rate of lightning strokes in 1000-km-radius region in the Caribbean is plotted for September 10, 2017. At the onset of the X8.2 flare at around 1600 UT, stroke rate drops 90% in a few minutes, and does not rise above the previous minimum recorded that day for several hours. We interpret this short-term decrease in stroke rate as sferics' inability to propagate out of the VLF attenuation region with sufficient power to be detected and used in lightning detection by WWLLN.

4 Conclusions

This analysis demonstrated the use of a global lightning detection network to map VLF attenuation in the EIWG caused by solar flares. Previous work has studied solar flare impact on low numbers of VLF transmitter-receiver paths, often only single paths (e.g. Bouderba, NaitAmor, & Tribeche, 2016). More recently, lightning detection networks have been used in conjunction with fixed VLF transmitters to study multi-path flare effects (Raulin, et al., 2010), and small numbers of receivers have probed the D-region ionosphere using lightning sferics as a VLF signal (Han & Cummer, 2010), (McCormick, Cohen, Gross, & Said, 2018). This work demonstrates global VLF attenuation mapping using a lightning detection network, with the ability to resolve equatorial attenuation features associated with solar flares.

The VLF attenuation mapped in this study has significant implications for the detection efficiency of WWLLN and other VLF lightning detection networks. WWLLN requires a minimum of 5 stations to detect a sferic in order to locate a lightning stroke; therefore, if multiple VLF propagation paths between a thunderstorm and

WWLLN stations are not viable due to increased low-altitude ionization, and the total number of WWLLN stations able to detect strokes from that thunderstorm falls below 5, WWLLN will be unable to detect those strokes. Strokes occurring inside VLF attenuation regions during X-class solar flares are unlikely to be detected, as demonstrated in Figure 4.

There are several shortcomings of this analysis that will be addressed in future work. First, the flares considered here are relatively "clean" and temporarily isolated events; that is, there are no flares of any significant magnitude preceding or following them by less than 1 hour, nor any other obvious sources of lower-ionosphere ionization enhancement (NOAA NCEI, 2019). Additionally, they are both very powerful, X-class events. As such, we expect them to produce a predictable and significant attenuation region on the day side lower ionosphere (Sauer & Wilkinson, 2008). Less powerful events may not produce attenuation that is as evident in a WWLLN stroke-station path analysis. So far, analyses of recent C-class flares (2 orders of magnitude less irradiance than X-class) have not shown an obvious attenuation effect on WWLLN sferics. Future work should address the lower limit on flare irradiance that is detectable as a single-event attenuation region, and perhaps the lower limit that is detectable in a superposed epoch analysis.

Second, this analysis relies on a 1-hour averaging threshold, chosen to fall between the timescales of flare onset (~1-10 minutes) and thunderstorm lifetime (hours) (Rakov & Uman, 2003). This threshold is effective at detecting attenuation produced at flare onset, especially when the hour preceding flare onset has relatively constant, low levels of X-ray irradiance. As soon as the flare occurs, however, the 1-hour average of stroke-station path crossings is disturbed, and as such the ionosphere recovery after peak flare irradiance cannot be effectively characterized by stroke-station path crossing differences. This could potentially be addressed with multiple averaging thresholds with different periods, or with the development of a no-flare path distribution prediction, which guesses the stroke-station path crossing distribution based on the pre-flare distribution of stroke-station paths and lightning, and a predicted lightning distribution that accounts for lightning strokes inside the attenuation region.

Finally, this work takes advantage of the globally-distributed nature of lightning strokes and WWLLN stations to provide adequate stroke-station path coverage over regions of interest. Unfortunately, sferic propagation is sparse over polar regions, due in part to the concentration of global lightning near the equator and mid-latitudes. Without increasing the number of stations in polar regions, this technique will be far more effective at characterizing equatorial VLF attenuation regions caused by solar flares than polar events associated with SEPs and CMEs.

In addition to addressing the shortcomings detailed above, this work is being developed into a real-time monitor of VLF attenuation in the EIWG. The WWLLN files needed for this analysis are available every 10 minutes, and the software used here runs in less than that time.

Acknowledgments

The authors would like to thank the World Wide Lightning Location Network, a collaboration among over 50 universities and institutions, for providing the lightning location data used in this work. These data are available at (doi:10.5281/zenodo.3598731), and upon request at https://wwlln.net. D-Region Absorption Prediction and GOES satellite data and plots are provided by the NOAA National Centers for Environmental Information (NCEI). D-RAP data are available at https://www.ngdc.noaa.gov/stp/drap/data/. GOES SEM data are available at https://www.ngdc.noaa.gov/stp/satellite/goes/dataaccess.html.
This work was internally funded by the University of Washington.

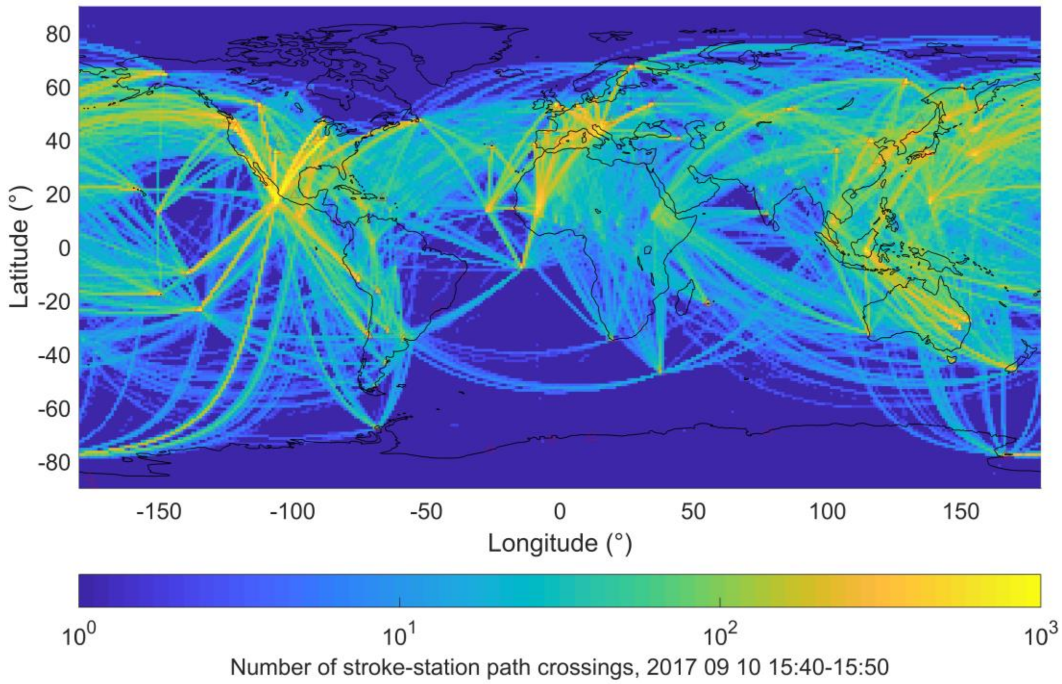

Figure 1. Sample WWLLN stroke-station distribution during a low-attenuation time, about 20 minutes before the X8.2 flare on September 10, 2017. WWLLN stations used in this analysis are marked with red triangles (Δ). Note that this distribution includes only integer values of stroke-station crossings, and the 10^0 minimum also includes cases of 0 stroke-station path crossings. Much of the dark blue regions in this figure, especially near the poles, have no stroke-station path crossings.

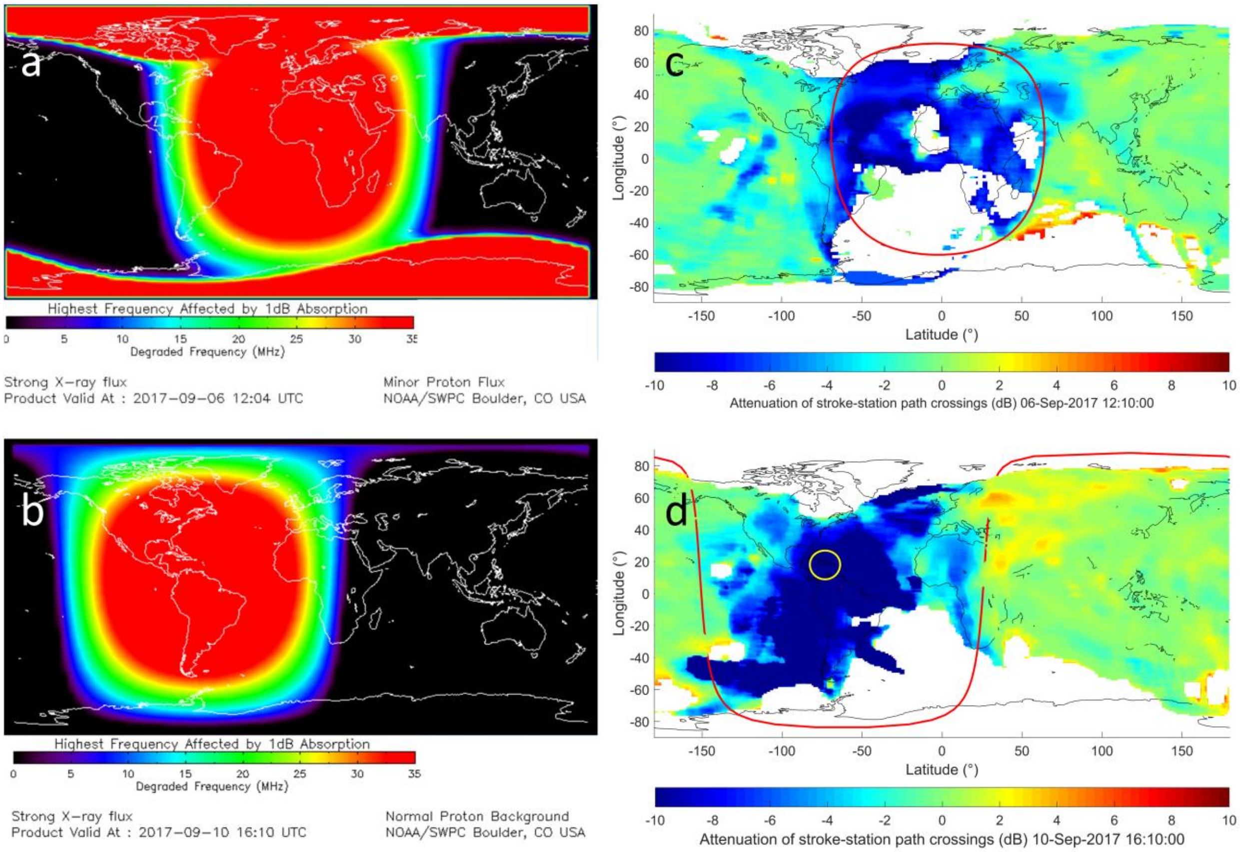

Figure 2. Comparison between D-RAP predicted HF attenuation region (left) and WWLLN stroke-station path attenuation (right) for the first 10 minutes of the September 6 X9.3 flare (top row) and the September 10 X8.2 solar flare (bottom row). Cooler colors in (c) and (d) correspond to attenuation of stroke-station paths, while warmer colors correspond to enhancement. The red circles in (c) and (d), centered on the sub-solar point, are the largest such circles enclosing a region of median attenuation above 6dB (see also Fig. 3). The yellow circle in (d) outlines a 1000-km-radius region in which WWLLN stroke count rate was analyzed; a time series of stroke count rate from this region is plotted in Figure 4. D-RAP maps are adapted from (NOAA NCEI, 2019)

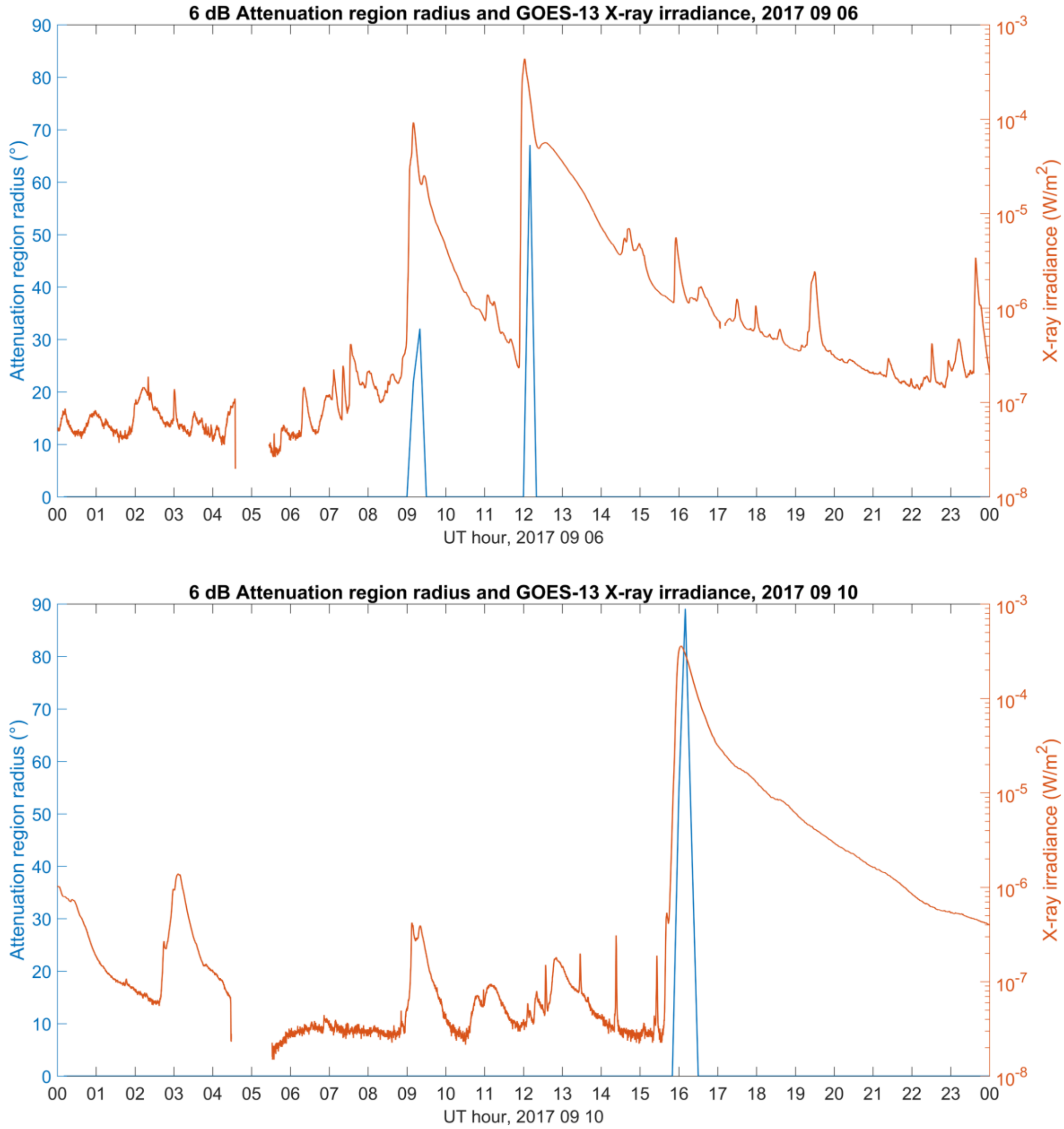

Figure 3. Comparison of 6-dB VLF attenuation region radius (blue, left axis) and GOES-13 0.05-0.4 nm X-ray irradiance (orange, right axis), for September 6 (top) and 10 (bottom). The blue curve is the radius, in degrees, of the largest circular subsolar region inside which the median stroke-station path attenuation is at least 6 dB. 6-dB regions are plotted as the red circles in Figure 2c and 2d; which correspond to the maxima of the blue curves in the upper and lower panels in this figure, respectively.

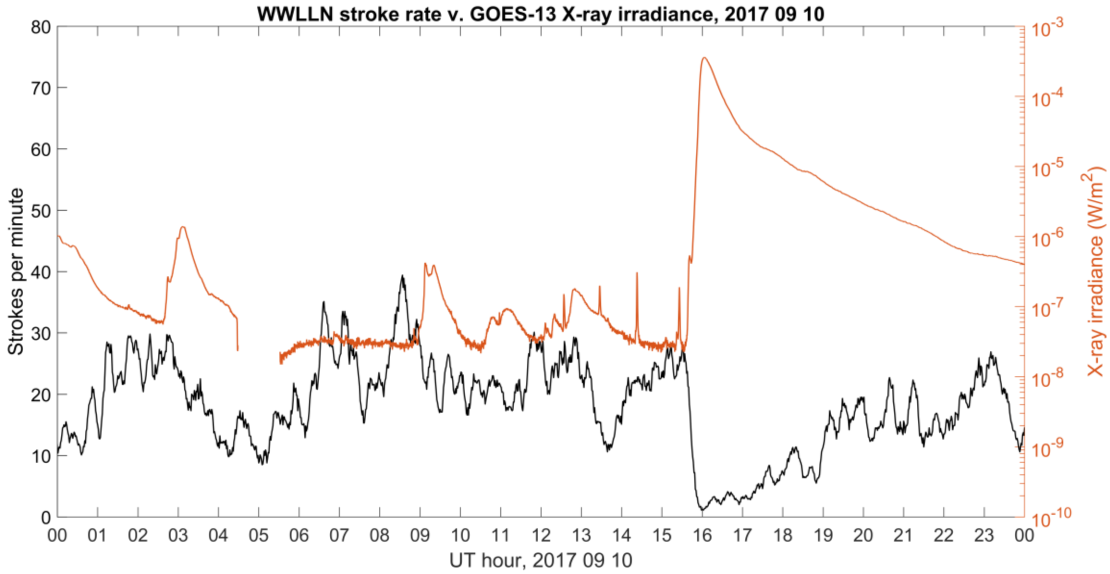

Figure 4. Comparison of WWLLN-detected lightning stroke count rate inside a near-subsolar region (black, left axis) and GOES-13 0.05-0.4 nm X-ray irradiance (orange, right axis). The region considered here is a 1000-km-radius area near the subsolar point, and is plotted as a yellow circle in Figure 2d. WWLLN detections of lightning strokes occurring within this region are plotted as the black curve. Stroke rate has been smoothed with a 10-minute moving average. At the onset of the X8.2 flare at around 1600 UT, WWLLN stroke rate inside this near-subsolar region drops an order of magnitude from around 25 to 2 strokes/minute.

References

Barr, R., Jones, D. L., & Rodger, C. J. (2000). ELF and VLF radio waves. *Journal of Atmospheric and Solar-Terrestrial Physics*, 1689-1718. doi:10.1016/S1364-6826(00)00121-8

Bouderba, Y., NaitAmor, S., & Tribeche, M. (2016). Study of the solar flares effect on VLF radio signal propagating along NRK-ALG path using LWPC code. *Journal of Geophysical Research: Space Physics*, 6799-6807. doi:10.1002/2015JA022233

Carvalho, F., Uman, M., Jordan, D., Hill, J., Cummer, S., Kotovsky, D., & Moore, R. (2017). Triggered lightning sky waves, return stroke modeling, and ionosphere effective height. *Journal of Geophysical Research: Atmospheres, 122*(6), 3507-3527. doi:10.1002/2016JD026202

Chilton, C. J., Steele, F. K., & Norton, E. B. (1963). Very-low-frequency phase observations of solar flare ionization in the D region of the ionosphere. *Journal of Geophysical Research*, 5421-5435. doi:10.1029/JZ068i019p05421

Codrescu, Mihail; NOAA Space Weather Prediction Center. (2010). *Global D-Region Absorption Prediction Documentation*. Retrieved from NOAA Space Weather Prediction Center: https://www.swpc.noaa.gov/content/global-d-region-absorption-prediction-documentation

Crombie, D. D. (1965). On the use of VLF measurements for obtaining information on the lower ionosphere (especially during solar flares). *Proceedings of the IEEE*, 2027-2034. doi:10.1109/PROC.1965.4479

Cummer, S., Inan, U., & Bell, T. (1998). Ionospheric D region remote sensing using VLF radio atmospherics. *Radio Science, 33*(6), 1781-1792. doi:10.1029/98RS02381

Dowden, R. L., Brundell, J. B., & Rodger, C. J. (2002). VLF lightning location by time of group arrival (TOGA) at multiple sites. *Journal of Atmospheric and Solar-Terrestrial Physics*, 817-830. doi:10.1016/S1364-6826(02)00085-8

Dowden, R. L., Holzworth, R. H., Rodger, C. J., Lichtenberger, J., Thomson, N. R., Jacobson, A. R., et al. (2008). World-Wide Lightning Location Using VLF Propagation in the Earth-Ionosphere Waveguide. *IEEE Antennas and Propagation Mag.*, 40-60. doi:10.1109/MAP.2008.4674710

Gary, D., Chen, B., Dennis, B., Fleishman, G., Hurford, G., Krucker, S., et al. (2018). Microwave and Hard X-Ray Observations of the 2017 September 10 Solar Limb Flare. *The Astrophysical Journal, 863*(1), 83. doi:10.3847/1538-4357/aad0ef

George, H. E., Rodger, C. J., Clilverd, M. A., Cresswell-Moorcock, K., Brundell, J. B., & Thomson, N. R. (2019). Developing a Nowcasting Capability for X-Class Solar Flares Using VLF Propagation Changes. *Space Weather*, 17. doi:10.1029/2019SW002297

Gołkowski, M., Sarker, S., Renick, C., Moore, R., Cohen, M., Kułak, A., et al. (2018). Ionospheric D Region Remote Sensing Using ELF Sferic Group Velocity. *Geophysical Research Letters*. doi:10.1029/2018GL080108

Gross, N., Cohen, M., Said, R., & Gołkowski, M. (2018). Polarization of Narrowband VLF Transmitter Signals as an Ionospheric Diagnostic. *Journal of Geophysical Research: Space Physics, 123*(1), 901-917. doi:10.1002/2017JA024907

Han, F., & Cummer, S. A. (2010). Midlatitude daytime D region variations measured from radio atmospherics. *Journal of Geophysical Research*, A10314. doi:10.1029/2010JA015715

Hutchins, M., Holzworth, R., Rodger, C., Brundell, J., Hutchins, M., Holzworth, R., et al. (2012). Far-Field Power of Lightning Strokes as Measured by the World Wide Lightning Location Network. *Journal of Atmospheric and Oceanic Technology*, *29*(8), 1102-1110. doi:10.1175/JTECH-D-11-00174.1

Jacobson, A., Holzworth, R., Lay, E., Heavner, M., & Smith, D. (2007). Low-frequency ionospheric sounding with Narrow Bipolar Event lightning radio emissions: regular variabilities and solar-X-ray responses. *Annales Geophysicae, 25*(10), 2175-2184.

Jacobson, A., Shao, X.-M., & Holzworth, R. (2010). Full-wave reflection of lightning long-wave radio pulses from the ionospheric D region: Comparison with midday observations of broadband lightning signals. *Journal of Geophysical Research: Space Physics, 115*(A5). doi:10.1029/2009JA014540

Levine, E. V., Sultan, P. J., & Teig, L. J. (2019). A Parameterized Model of X-Ray Solar Flare Effects on the Lower Ionosphere and HF Propagation. *Radio Science*, 168-180. doi:10.1029/2018RS006666

Markowski, P., & Richardson, Y. (2011). *Mesoscale Meteorology at the Midlatitudes.* Wiley Blackwell.

McCormick, J., Cohen, M., Gross, N., & Said, R. (2018). Spatial and Temporal Ionospheric Monitoring Using Broadband Sferic Measurements. *Journal of Geophysical Research: Space Physics, 123*(4), 3111-3130. doi:10.1002/2017JA024291

Mitra, A. P. (1974). *Ionospheric Effects of Solar Flares.* D. Reidel .

NOAA NCEI. (2019). *D-Region Absorption Prediction Product Archive*. Retrieved from NOAA National Centers for Environmental Information Space Weather Data Archive: https://www.ngdc.noaa.gov/stp/drap/index.html

NOAA NCEI. (2019). *GOES Space Environment Monitor Data and Documentation*. Retrieved from NOAA National Centers for Environmental Information Space Weather Data Archive: https://www.ngdc.noaa.gov/stp/satellite/goes/index.html

Parks, G. K. (2004). *Physics of space plasmas.* Cambridge: Westview Press.

Qian, L., Wang, W., Burns, A., Chamberlin, P., Coster, A., Zhang, S.-R., & Solomon, S. (2019). Solar Flare and Geomagnetic Storm Effects on the Thermosphere and Ionosphere During 6–11 September 2017. *Journal of Geophysical Research: Space Physics, 124*(3), 2298-2311. doi:10.1029/2018JA026175

Rakov, V. A., & Uman, M. A. (2003). *Lightning: Physics and Effects.* Cambridge: Cambridge University Press.

Raulin, J.-P., Bertoni, F., Gavilán, H., Guevara-Day, W., Rodriguez, R., Fernandez, G., et al. (2010). Solar flare detection sensitivity using the South America VLF Network (SAVNET). *Journal of Geophysical Research: Space Physics, 115*(A7). doi:10.1029/2009JA015154

Sauer, H., & Wilkinson, D. (2008). Global mapping of ionospheric HF/VHF radio wave absorption due to solar energetic protons. *Space Weather, 6*(12). doi:10.1029/2008SW000399

Siingh, D., Gopalakrishnan, V., Singh, R. P., Kamra, A. K., Singh, S., Pant, V., et al. (2007). The atmospheric global electric circuit: an overview. *Atmospheric Research*, 91-110. doi:10.1016/j.atmosres.2006.05.005

Thomson, N. (1993). Experimental daytime VLF ionospheric parameters. *Journal of Atmospheric and Terrestrial Physics, 55*(2), 173-184. doi:10.1016/0021-9169(93)90122-F

Thomson, N. R., & Clilverd, M. A. (2001). Solar flare induced ionospheric D-region enhancements from VLF amplitude observations. *Journal of Atmospheric and Solar-Terrestrial Physics*, 1729-1737. doi:10.1016/S1364-6826(01)00048-7

Uman, M. A., & Krider, E. P. (1982). A Review of Natural Lightning: Experimental Data and Modeling. *IEEE Transactions on Electromagnetic Compatibility*, 72-112. doi:10.1109/TEMC.1982.304006

Volland, H. (Ed.). (1995). *Handbook of Atmospheric Electrodynamics* (Vol. 2). Boca Raton: CRC Press.

Wenzel, D., Jakowski, N., Berdermann, J., Mayer, C., Vallardes, C., & Heber, B. (2016). Global ionospheric flare detection system (GIFDS). *Journal of Atmospheric and Solar-Terrestrial Physics*, 233-242. doi:10.1016/j.jastp.2015.12.011

Westerlund, S., & Reder, F. H. (1973). VLF radio signals propagating over the Greenland ice-sheet. *Journal of Atmospheric and Terrestrial Physics*, 1475-1491. doi:10.1016/0021-9169(73)90149-9

Yasyukevich, Y., Astafyeva, E., Padokhin, A., Ivanova, V., Syrovatskii, S., & Podlesnyi, A. (2018). The 6 September 2017 X-Class Solar Flares and Their Impacts on the Ionosphere, GNSS, and HF Radio Wave Propagation. *Space Weather, 16*(8), 1013-1027. doi:10.1029/2018SW001932